ce/papers
The online collection for conference papers in civil engineering
Ernst & Sohn A Wiley Brand

ORIGINAL ARTICLE

eurosteel SHEFFIELD 2021
Ernst & Sohn A Wiley Brand

Stability Study of Cantilever-Beams – Numerical Analysis and Analytical Calculation (LTB)

Matthias Kraus, Nicolae-Andrei Crișan, Björn Wittor

Correspondence

Prof. Dr. Matthias Kraus
Bauhaus University of Weimar,
Chair of Steel and Hybrid Structures,
Marienstraße 13D,
Germany, 99423 Weimar
matthias.kraus@uni-weimar.de

Abstract

According to Eurocode, the computation of bending strength for steel cantilever beams is a straightforward process. The approach is based on an Ayrton-Perry formula adaptation of buckling curves for steel members in compression, which involves the computation of an elastic critical buckling load for considering the instability. NCCI documents offer a simplified formula to determine the critical bending moment for cantilevers beams with symmetric cross-section. Besides the NCCI recommendations, other approaches, e.g. research literature or Finite-Element-Analysis, may be employed to determine critical buckling loads. However, in certain cases they render different results. Present paper summarizes and compares the abovementioned analytical and numerical approaches for determining critical loads and it exemplarily analyses corresponding cantilever beam capacities using numerical approaches based on plastic zones theory (GMNIA).

Keywords

stability, buckling, analytical, Eurocode, FEM, plastic zones theory

1 Introduction

Lateral-torsional buckling (shortly, LTB) is the main failure mode of steel beams loaded in the plane of the weak axis effected by the economical use of material. It is a structural instability that causes the loaded member to deflect and twist out of the loading plane. A common form of LTB is observed for I-section beams which are loaded in their web plane, but which buckle by deflecting laterally out of that plane and twisting about its longitudinal axis [1], as presented in Figure 1.

The initial theoretical research was preceded by Euler's 1759 treatise [2] on column flexural buckling which gave the first analytical method of predicting reduced strengths of slender columns. More than 100 years later, Michell [3] and Prandtl [4] published first treatments of LTB. Their work was further extended by Timoshenko [5], [6] to include effects of warping torsion of I-section beams. Regarding practical applications, Chwalla [7] obtained siginficantly improved solutions.

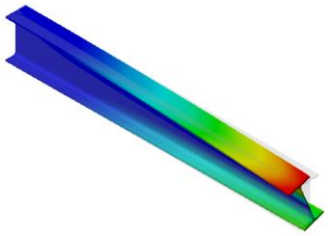

Figure 1 Lateral-torsional buckling of a cantilever I beam

Lateral-torsional buckling was the subject of many research projects, but prior to the 1960s, these were limited by the necessity to make extensive calculations by hand. Once the general finite element method (FEM) was extended to structural analysis, almost any situation could have been analysed using a general-purpose computer program. The employment of numerical methods opened the study of LTB using numerical approaches such as finite integral, finite difference, finite element and finite strips methods [8]. In case of different boundary conditions or load types, the moment gradient is not constant and analytical solutions are either too complex or involve infinite series.

The need to be able to design against lateral-torsional buckling was the catalyst for the development of a theory which would allow the successful prediction of failure. Some of the early well-documented experiments on lateral buckling of steel beams were carried out by Hechtman, Hattrap, Styer, and Tiedmann [9] for instance. Fukumoto and Kubo [10-12] reviewed and produced a data base of the experimental studies on lateral buckling of steel beams.

2 Design procedure with reduction factors for steel beams

In accordance to EN1993-1-1 [13] design procedure, the bending moment capacity of a steel beam made of an I-profile is given by the following formula:

$$M_{b,Rd} = \chi_{LT} \cdot W_y \cdot \frac{f_y}{\gamma_{M1}} \quad (1)$$

The moment capacity of the cross section $W_y \cdot f_y$ is adjusted by the

reduction factor χ_{LT} incorporating lateral torsional buckling influence into the structural behaviour of the member. For determining the reduction factor, a corresponding perfect member, i.e. a member without any imperfections (e.g. residual stresses or geometric imperfections), is observed first, considering an unlimited elastic material behaviour. The capacity of that perfect member is expressed by the elastic critical moment M_{cr}, which is the stress under which the member leaves the state of stable equilibrium. Using a non-dimensional slenderness (based on the cross section capacity as well as M_{cr}) to express the sensitivity of the perfect member regarding stability, the capacity of a corresponding "real" member going along with the same slenderness is determined in terms of χ_{LT}:

$$\bar{\lambda}_{LT} = \sqrt{\frac{W_y \cdot f_y}{M_{cr}}} \tag{2}$$

$$\chi_{LT} = \frac{1}{\phi_{LT} + \sqrt{\phi_{LT}^2 - \beta \cdot \bar{\lambda}_{LT}^2}} \quad \leq \begin{cases} 1.0 \\ 1/\bar{\lambda}_{LT}^2 \end{cases} \tag{3}$$

$$\text{with} \quad \phi_{LT} = 0.5 \cdot [1 + \alpha_{LT} \cdot (\bar{\lambda}_{LT} - \bar{\lambda}_{LT,0}) + \beta \cdot \bar{\lambda}_{LT}^2] \tag{4}$$

Different profiles and associated imperfections yield in different capacities and thus χ_{LT}, which is captured by the imperfection factor α_{LT} leading to different lateral torsional buckling curves as shown in Figure 2. EN 1993-1-1 specifies imperfection factors of 0.34, 0.49, and 0.76 for different rolled and welded I-profiles. The reference slenderness parameter $\bar{\lambda}_{LT,0}$ limits the plateau length of the lateral torsional buckling curves, i.e. it gives a boundary value of the non-dimensional slenderness up to which lateral torsional buckling does not impact the capacity of the member. EN 1993-1-1 recommends a value of 0.4 for $\bar{\lambda}_{LT,0}$. The coefficient $\beta = 0.75$ corrects the lateral torsional buckling curves with respect to rolled and welded I sections.

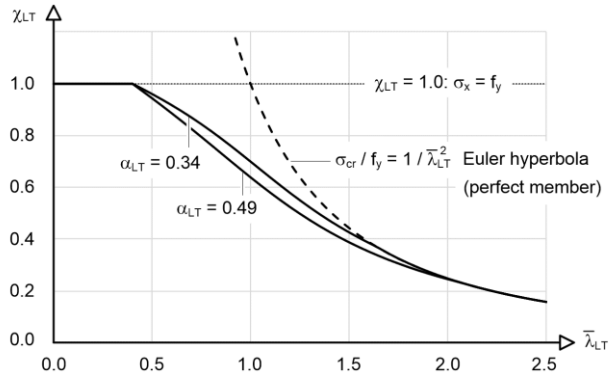

Figure 2 Examples of lateral torsional buckling curves

The factor χ_{LT} in Equation (3) describes the capacity of a member based on a uniform moment distribution, which is the most unfavourable case. It may be modified to a beneficial value $\chi_{LT,mod}$, in case a different moment distribution stresses the member. Details can be taken from [13].

3 Determination of elastic critical moments M_{cr}

3.1 Introduction

Within the design procedure of Eurocode, a major task is the determination of the elastic critical moment M_{cr}. However, the design code provides no further provisions regarding the computation. M_{cr} reflects the capacity of a perfect member, i.e. the bending moment under which the member is not at stable equilibrium, considering unlimited elastic material behaviour and not taking any imperfections into account. Since this does not reflect structural conditions of "real" members and beams do not provide post critical reserves, M_{cr} will always be larger than the moment capacity $M_{b,Rk}$. Next to properties of the member, which may in terms of torsion be captured by the member characteristic

$$\varepsilon_T = L \cdot \sqrt{GI_T / EI_\omega}, \tag{5}$$

the boundary conditions as well as the loads and the position of their acting have decisive influence on M_{cr}. In Equation (5), L denotes the member length, GI_T the torsional rigidity and EI_ω the warping stiffness (with *St. Venants* torsional constant I_T and warping constant I_ω). If member characteristics ε_T provide large values, load is carried by primary torsional stress states (*St. Venants* torsion, pure shear stress state). For small values of ε_T, loads are mainly carried by secondary torsion (axial and shear stress state). For I-cross sections, ε_T is usually in a range where combined states, i.e. primary and secondary torsional stress states referred to as warping torsion, contribute to the state of equilibrium.

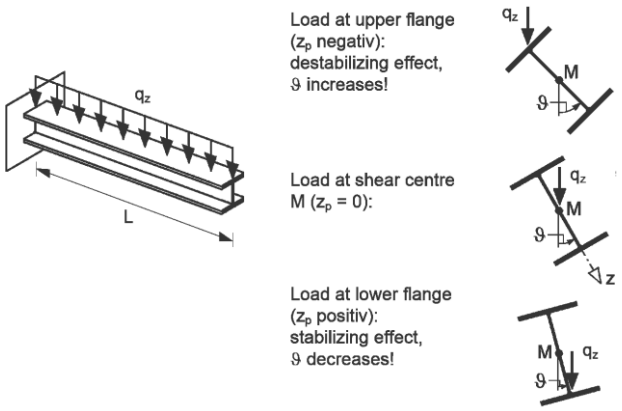

Figure 3 Influence of position of load application

As mentioned above and shown in Figure 3, the position of load application has decisive influence on the carrying behaviour of members susceptible to lateral torsional buckling and therefore on the critical moment complicating analytical treatment. It is therefore state of the art to apply numerical procedures (e.g. FEM) to determine M_{cr}. Formulating the eigenvalue problem with the homogeneous equation system

$$(\underline{K} + \alpha_{cr} \cdot \underline{G}) \cdot \underline{v} = 0 \tag{6}$$

allows determining the smallest positive eigenvalue α_{cr} (critical loading factor) of a structural system and the eigenvector $\underline{v}$ representing the mode shape of the system. $\underline{K}$ is the stiffness matrix and $\underline{G}$ the geometric stiffness matrix capturing influences of geometric nonlinearities (second order theory). Using the critical loading factor, the critical moment is determined by

$$M_{cr} = \alpha_{cr} \cdot M, \tag{7}$$

where M is the bending moment stressing the structural system. Details on FEM regarding steel structures and the solution of eigenvalue problems are found in [14].

However, different analytical approximations of M_{cr} are also available in literature for practical applications of rather simple structural systems. Since the preciseness of these solutions is in general unclear and formulae are edited differently, even though they have a common origin, the following sections are supposed to give certain overview for cantilevers with distributed loads as shown in Figure 3. Furthermore, the majority of design examples found in literature are based on simply supported beams, see [15] for example.

3.2 NCCI [16, 17]

A well-known formula for practical applications regarding M_{cr}, which was part of a pre-version of EN 1993 for example, is given by:

$$M_{cr} = C_1 \frac{\pi^2 \cdot EI_z}{L^2} \cdot \left[\sqrt{c^2 + \left(C_2 z_p\right)^2} + C_2 z_p \right] \tag{8}$$

with $c^2 = \frac{I_\omega}{I_z} + \frac{L^2 \cdot GI_T}{\pi^2 \cdot EI_z}$

This equation has also been picked up in NCCI document [16] in a slightly adjusted manner. The basis for deriving Equation (8) is a single span girder with fork bearings at beam ends and a constantly distributed load. Formulating equilibrium based on energy methods with respect to lateral torsional buckling and solving the eigenvalue problem leads to the formula, when for lateral displacements v and torsional rotations ϑ a single waved sine alternation as displacement approach is introduced. Details are given in [18] for example. In case of the single span girder with uniformly distributed load, $C_1 = 1.12$ and $C_2 = 0.45$. Since Equation (8) may in general be derived for other structural systems as well, it can be applied properly by adjusting C_1 and C_2 with respect to different load situations and boundary conditions. In the past, corresponding factors have been determined using analytical investigations and especially solutions of numerical calculations. However, analyses of the authors have shown that especially C_2 leads to quite extensive analytical formulations when applied to cantilever beams, see [19] as well.

Table 1 C-factors for cantilevers with constantly distributed load and warping restraint at support [17]

	η						
κ_{wt}	1	0.5	0	-0.25	-0.5	-0.75	-1
0	2.04	2.04	2.04	2.04	2.04	2.04	2.04
0.05	2.61	2.5	2.39	2.33	2.27	2.21	2.15
0.1	3.33	3.07	2.8	2.65	2.51	2.36	2.22
0.15	4.15	3.72	3.23	2.97	2.71	2.47	2.23
0.2	5.03	4.42	3.68	3.28	2.89	2.53	2.22
0.3	6.91	5.93	4.57	3.82	3.14	2.59	2.16
0.4	8.87	7.52	5.45	4.29	3.32	2.62	2.13
0.6	12.9	10.8	7.15	5.1	3.65	2.74	2.17
0.8	17	14.2	8.85	5.92	4.05	2.98	2.33
1	21.1	17.6	10.6	6.8	4.54	3.3	2.57

This explains a subsequent NCCI document [17] providing support for determining the critical buckling load for cantilever beams:

$$M_{cr} = \frac{k}{L} \sqrt{EI_z \cdot GI_T} \quad \text{with} \quad k = C \cdot \pi \tag{9}$$

The factor C is specified in [17] for selected cases. Table 1 gives overview for cantilever beams with full warping restraint at the support and constantly distributed load. The influence of the position of load application and the member characteristic is incorporated as shown in Figure 4 by:

$$\eta = \frac{2 \cdot z_p}{h_f} \tag{10}$$

$$\kappa_{wT} = \frac{1}{\varepsilon_T} \tag{11}$$

To be consistent in formulations, the sign of η has been changed here in comparison to [17].

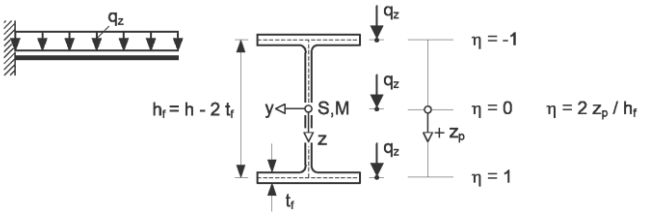

Figure 4 Definition of the position of load application

At first sight, the correspondence of Equations (8) und (9) is not directly recognizable. However, when the point of load application is assumed to be in the shear centre M (falling together with the centroid S for doubly symmetric cross sections), i.e. $z_p = 0$, Formula (8) can be reformed as follows:

$$M_{cr} = C_1 \frac{\pi^2 \cdot EI_z}{L^2} \cdot \sqrt{c^2} \tag{12}$$

$$\Rightarrow M_{cr}^2 = C_1^2 \cdot EI_z \cdot GI_T \cdot \left(\frac{\pi^2}{L^2} + \frac{\pi^4 \cdot EI_\omega}{L^4 \cdot GI_T} \right)$$

$$\Rightarrow M_{cr} = \frac{k}{L} \sqrt{EI_z \cdot GI_T} \quad \text{with} \quad k = C_1 \cdot \pi \cdot \sqrt{1 + \pi^2 / \varepsilon_T^2} \tag{13}$$

As can be seen, Formula (9) is closely related to Equation (13) and thus to Equation (8), respectively, based on a corresponding theoretical background.

3.3 DIN 4114 [20]

A former German national standard for the stability of members is DIN 4114 [20]. It provides the formula stated in Equations (9) and (13), respectively,

$$M_{cr} = \frac{k}{L} \sqrt{EI_z \cdot GI_T}, \tag{14}$$

where the factor k for different load situations is specified in the diagrams of Figure 5.

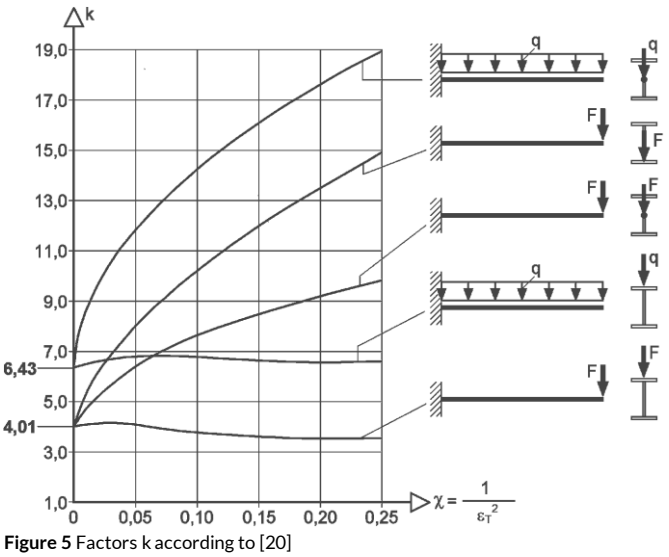

Figure 5 Factors k according to [20]

3.4 AISC [21]

For lateral-torsional buckling of doubly symmetric cross-sections the following formula is given in [21]:

$$M_{cr} = C_b \cdot \frac{\pi}{L}\sqrt{EI_z \cdot GI_T + \left(\frac{\pi \cdot E}{L}\right)^2 \cdot I_z \cdot I_\omega} \tag{15}$$

For reasons of consistency, some notations have slightly been adjusted here. Besides the indication that for cantilevers where warping is prevented at the support and where the free end is unbraced, $C_b = 1.0$, no further indications are given.

Considering the member characteristic (5), Equation (15) may be reformed as follows:

$$M_{cr}^2 = C_b^2 \cdot EI_z \cdot GI_T \cdot \left(\frac{\pi^2}{L^2} + \frac{\pi^4 \cdot EI_\omega}{L^4 \cdot GI_T}\right)$$

$$\Rightarrow M_{cr} = \frac{k}{L}\sqrt{EI_z \cdot GI_T} \quad \text{with} \quad k = C_b \cdot \pi \cdot \sqrt{1 + \pi^2/\varepsilon_T^2} \tag{16}$$

This formulation is identical to Equation (13). Therefore Equation (15) also corresponds to Equation (8), if load is assumed to be acting at the shear centre. As can be seen, Formula (15) is closely related to the NCCI approach for cantilevers (9) and the one of DIN 4114 (14) as well, with the big difference, that with the definition of the single value $C_b = 1.0$ the influence of the load position is not specifically taken account of.

3.5 Comparison of NCCI, DIN 4114, and AISC

The previous sections show that different calculation formulae for M_{cr} may be revised to an identical expression:

$$M_{cr} = \frac{k}{L}\sqrt{EI_z \cdot GI_T} \tag{17}$$

However, by doing so the approaches provide slight difference in the facors k, which is exemplified for cantilevers with constantly distributed load and a full warping restraint at the support in this section.

Table 2 Critical moments M_{cr} [kNm] of cantilevers with distributed load determined with FEM (beam theory)

		η (z_p in cm)				
		1.0	**0.5**	**0.0**	**-0.5**	**-1.0**
1/εT	**L [cm]**	(9.575)	(4.788)	(0.0)	(-4.788)	(-9.575)
0.05	1390	24.18	23.16	22.10	21.01	19.90
0.10	694.8	61.73	56.99	51.78	46.33	40.93
0.15	463.2	115.4	103.6	89.76	75.12	61.63
0.20	347.4	186.7	164.2	136.2	106.4	81.42
0.30	231.6	384.9	330.4	254.0	173.3	118.7
0.40	173.7	659.1	559.0	403.5	243.6	155.1
0.60	115.8	1439	1207	794.5	400.4	236.5
0.80	86.85	2528	2113	1311	592.2	338.6
1.00	69.48	3929	3276	1959	828.0	465.9

For reasons of comparison, solutions of finite element calculations using the software FE-STAB are displayed as well. The program is based on beam theory and able to describe warping torsion with respect to second order theory, see Figure 11, which shows the degrees of freedom. The numerical analyses were performed using an IPE 200 with torsional cross section properties of $I_T = 6.846\ cm^4$ and $I_\omega = 12{,}746\ cm^6$, which are precise properties taking rolling fillets into account, see [22, 23]. In order to capture the influence of the member characteristic ε_T, member lengths were adjusted accordingly. Table 2 gives overview on the critical moments determined with FE-STAB for different load application points.

The k factors of the different approaches regarding the computation of M_{cr} are shown in Figure 6. As can be seen, the values computed according to NCCI fit to the numerical results very well with a maximum deviation of approximately 1.6%. This does not surprise, as C values of NCCI were derived using numerical approaches as well. From a practical point of view, the k factors stated in DIN 4114 also show good agreement to the numerical results. The approach of AISC with only stating one value of $C_b = 1.0$ is quite conservative up to approximately $1/\varepsilon_T = 0.6$ and thus partially uneconomic. However, for roughly $1/\varepsilon_T > 0.6$ and load application at the upper flange, the indications of AISC give unsafe estimations.

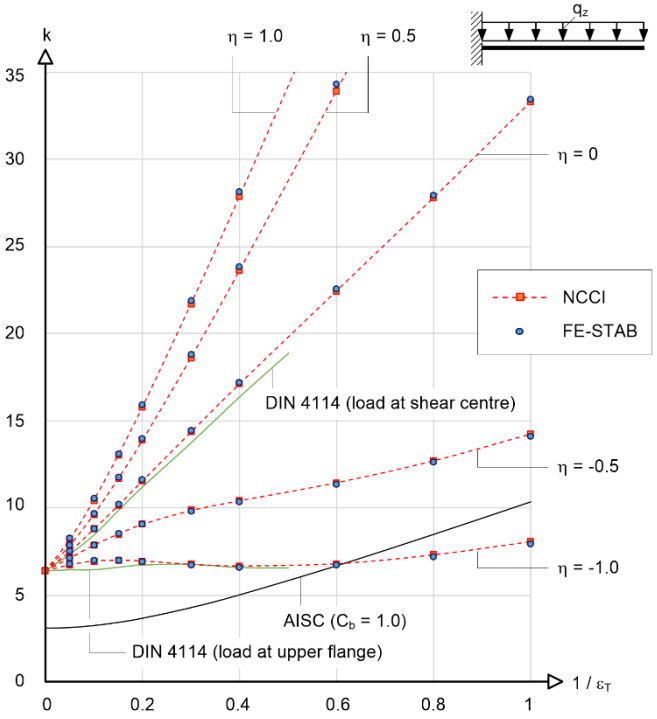

Figure 6 Comparison of factors k based on different calculation approaches

3.6 Extended Formulae

It is worth mentioning that Ozbasaran et al. [24] present a procedure for LTB of cantilever I-beams. First a closed-form equation based on energy method is proposed to determine elastic critical loads of singly and doubly symmetric cantilever I-beams which considers the effect of the distance between acting point of the load and shear centre of the section. Further, taking advantage of experimental data and analytical solutions, the calculation of the critical moment of cantilever I-beams is proposed as follows:

$$\frac{M_{cr}}{L} = \frac{\sqrt{EI_z}}{2D_4L^3}\left[\sqrt{4D_4(D_3C_1 + D_1CL^2) + EI_z(D_5H_A + D_2\beta_x)^2} - \sqrt{EI_z}(D_5H_A + D_2\beta_y)\right] \tag{18}$$

with $C = GI_T$, $C_1 = EI_\omega$ and $\beta_y = \frac{1}{I_y}\int_A z(y^2 + z^2)dA$

Parameters D_i are obtained by numerical solution of the governing differential equation with respect to ε_T. It's worth mentioning that for bisymmetric I sections, it is $\beta_y = 0$.

[19] also presents deep investigations and formulae including singly symmetric cross sections as well, which are quite extensive with regard to practical application. However, as shown in the previous section, the approach of NCCI using the simpler Formula (17) already provides very good approximation of critical moments for cantilever beams. Since the corresponding C-factors are defined for selected cases only, different applications may be connected to interpolations along with an increased effort. For that reason Equation (17) is extended here using the following approach:

$$M_{cr} = \frac{k_1}{L}\sqrt{EI_z \cdot GI_T} \cdot (1 + k_2) \tag{19}$$

The factor k_2 is supposed to capture influences of the point of load application. In case the load is acting in the shear centre, k_2 is to be zero. Using this condition, factor k_1 may be determined in a first step by adjusting it to the numerical results of Table 2 considering the case $\eta = 0$. Figure 6 shows the emerging function $k = k_1$ depending on the member characteristic. As can be seen, the curve for $\eta = 0$ is nearly a linear function, which can be described well as follows:

$$k_1 = 6.18 + 27.3/\varepsilon_T \tag{20}$$

In a second step, an approximation for k_2 is to be found. Examining Figure 6 gives conclusion that the influence of load application leads to strong differing functional courses. On the basis of analytical formulations, k_2 results in a quite extensive formulation unfavourable for practical applications. For that reason, factors k_2 fitting the critical moments of the numerical results of Table 2 were determined. They are displayed in Figure 7 as blue dots. Using a non-linear fitting in terms of regression analysis on the basis of a bi-cubic polynomial function and optimizing arising polynomials gives the following function:

$$k_2 = \eta\left(\frac{2.33-0.195\eta}{\varepsilon_T} + \frac{0.686\eta-1.64\eta^2-0.602}{\varepsilon_T^2} + \frac{1.17\eta^2-0.365\eta-0.363}{\varepsilon_T^3}\right) \tag{21}$$

The plane described with this functional course is displayed in Figure 7 as well. As can be seen, it fits the factors based on the numerical results (blue dots) very well. Regarding M_{cr}, discrepancies of Equations (19) to (21) in comparison to the numerical results of Table 2 are in general smaller than 1%. Single values are a bit larger, the under and overestimation observed are 3.8% and 1.9% at maximum.

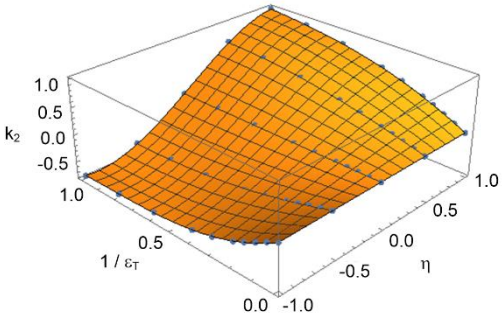

Figure 7 Factors k_2 based on numerical results (blue dots) and fitted functional course of Equation (21)

However, for practical applications Equation (21) is also connected with certain effort. Since $\eta = 1$ (load a lower flange) as well as $\eta = -1$ (load at upper flange) are of particular importance in that context, Equation (20) may be simplified for these cases as follows:

$$\eta = 1: \quad k_2 = \frac{2.131}{\varepsilon_T} - \frac{1.560}{\varepsilon_T^2} + \frac{0.4375}{\varepsilon_T^3} \tag{22}$$

$$\eta = -1: \quad k_2 = -\frac{2.522}{\varepsilon_T} + \frac{2.932}{\varepsilon_T^2} - \frac{1.168}{\varepsilon_T^3} \tag{23}$$

As an example, a HEA 240 profile ($I_z = 2{,}769\ cm^4$, $I_T = 41.03\ cm^4$, and $I_\omega = 321{,}640\ cm^6$) of $L = 200\ cm$ length and load at the upper flange ($\eta = -1$) is considered. This gives $\varepsilon_T = 1.403$ and with Equations (20) and (23) $k_1 = 25.6$ and $k_2 = -0.731$. Inserted in Equation (19) leads to:

$$M_{cr} = \frac{25.6}{L}\sqrt{EI_z \cdot GI_T} \cdot (1 - 0.731) = 1514\ kNm$$

For comparison, a calculation with the finite element program FE-STAB gives $M_{cr} = 1533\ kNm$, which is approximated very well (1% discrepancy). If, for academic purpose, $\eta = -0.3$ is assumed, $k_2 = -0.349$ using Equation (21). With this it is:

$$M_{cr} = \frac{25.6}{L}\sqrt{EI_z \cdot GI_T} \cdot (1 - 0.349) = 3663\ kNm$$

Here, a calculation of FE-STAB results in $M_{cr} = 3545\ kNm$ deviating by approximately 3%.

3.7 Sophisticated FEM-model

In the previous sections, critical moments were determined according to beam theory using analytical and numerical methods (FEM), as this is the common practice for the application of design rules in EN 1993-1-1 depicted in chapter 2. Regarding the solutions of Table 2, finite beam elements with 7 degrees of freedom (3 translations, 3 rotations and the derivate of angle of torsional twist capturing warping torsion) were considered, see Figure 11. Here, these solutions are to be compared to results based on Equation (6) applying sophisticated three-dimensional finite element models using the commercial software ANSYS. For that purpose, volume elements according to Figure 9 were considered in the model of the cantilever and different meshes were studied in terms of solution convergence.

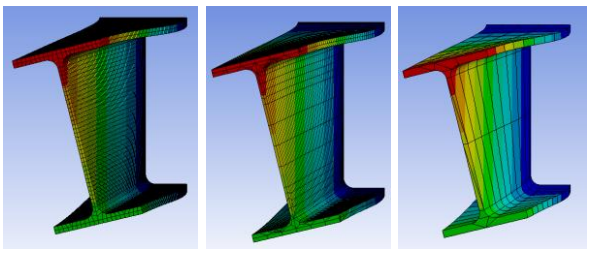

Figure 8 First eigenmode of a cantilever beam with three different mesh-qualities

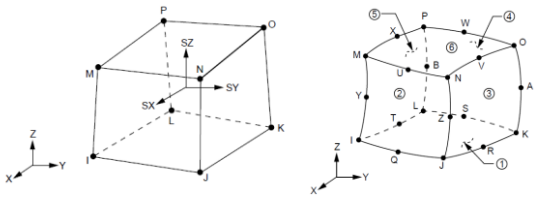

Figure 9 Solid-Elements used in ANSYS: 8 nodes solid element (left), 20 nodes quadratic solid element (right) [25]

Figure 8 exemplary shows three different mesh qualities in that context. The Mesh size and quality decreases from the left to the right model. The quality of results strongly depends on input parameters and insufficient mesh qualities or an inappropriate selection of elements may lead to strong deviations and very inaccurate results. Figure 10 gives an overview on the influence of the mesh size and

the usage of quadratic instead of linear elements. The use of linear elements reduces calculation time; however, for good results a finer mesh is necessary. In the studied case, the quadratic elements (20-nodes) also give for coarse meshes good results in terms of critical moments.

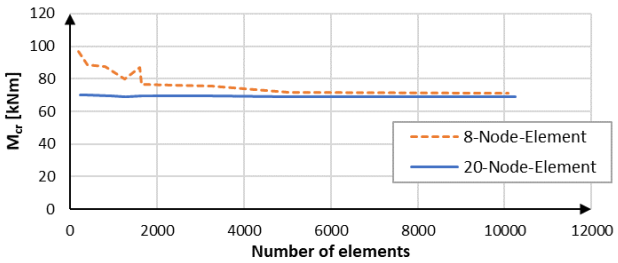

Figure 10 Critical moments calculated with ANSYS in dependency of the mesh size and the element-formulation

Applying the best mesh quality, a parameter analyses corresponding to the previous calculations was conducted. By comparing critical moments of the sophisticated FEM-simulation using volume elements with results using beam elements in Table 2, the following congruence is detected:

$\frac{1}{\varepsilon_T} \leq 0.2$: Deviation to beam model <2%

$\frac{1}{\varepsilon_T} \leq 0.4$: Deviation to beam model <10%

$\frac{1}{\varepsilon_T} > 0.4$: strong deviations due to local buckling influences

For short beams with $1/\varepsilon_T > 0.4$, the eigenmodes corresponding to the smallest positive eigenvalues include effects of local buckling interfering with the global mechanism. In these cases, a comparison to results of beam theory is not useful. As can be seen, the sophisticated models lead to predictions of critical moments close to solutions of beam theory. Expectedly, the more distinctive a beam is (in terms of cross section size to beam length), the better the correspondence gets. However, the analyses also show, that the effort of modelling and determining meaningful results with more sophisticated approaches than beam elements is extremely high with no significant advantage regarding practical applications in the context of lateral torsional buckling. The only benefit is insight, whether local buckling influences may be of importance regarding beam capacities. If eigenmodes of complex models are clearly identified as modes of lateral torsional buckling not influenced by local mechanisms, corresponding elastic critical moments may certainly be introduced in calculation process of EN 1993-1-1 leading to reliable approximations of resistance.

4 Examples of cantilever beam resistance based on different approaches

4.1 Resistance based on plastic zones theory

This chapter focuses on member capacity of cantilever beams. For that purpose, different calculations are exemplarily presented. In a first step, an approach based on plastic zones theory is followed, i.e. geometrically and materially nonlinear analyses including imperfections (GMNIA) based on beam theory. In terms of EN 1993, the investigations are to be classified as plastic structural analysis taking local plasticising into account. Suchlike calculations are able to predict the structural behaviour of members very well [26] and allow for a much better interpretation of results in comparison to simplified approaches based on reduction factors presented in chapter 2.

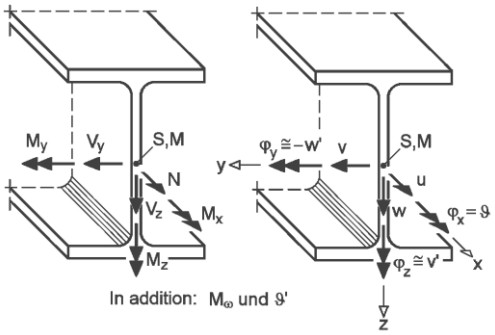

Figure 11 Internal forces and moments as well as degrees of freedom

In general the plastic zones theory is based on iterative and incremental procedures where loads are increased until the capacity of the structure is reached. This may be due to reasons of plastic mechanisms (plastic capacity of cross section is fully utilized), or, which is more likely for members susceptible to lateral torsional buckling, that the eigenvalue of a partially plasticized member is reached due to load increase, i.e. the structure is not at stable equilibrium anymore. As solution of the numerical analysis, the ultimate (limit) load factor α_{ult} is depicted, which describes, how much loads may be increased to reach the ultimate limit state (capacity) of the member.

The calculations based on plastic zones theory are performed using the program FE-STAB-FZ, which is an extension of the previously mentioned and applied FE-STAB (elastic analyses) with regard to physical nonlinearity implemented by *Laumann/Wolf/Kindmann*. It uses the theoretical background based on beam theory substantially provided in [14] and [27], respectively. The corresponding finite elements capture biaxial bending with warping torsion. The internal forces and moments together with the incorporated degrees of freedom are shown in Figure 11. The notation for the torsional moment is M_x and for the warping bi-moment M_ω. Regarding displacements, ϑ is the torsional rotation about the longitudinal beam axis x, ϑ' the derivate of angle of twist going along with the warping of the cross-section, and v the lateral displacement in direction of the principal cross section axis y.

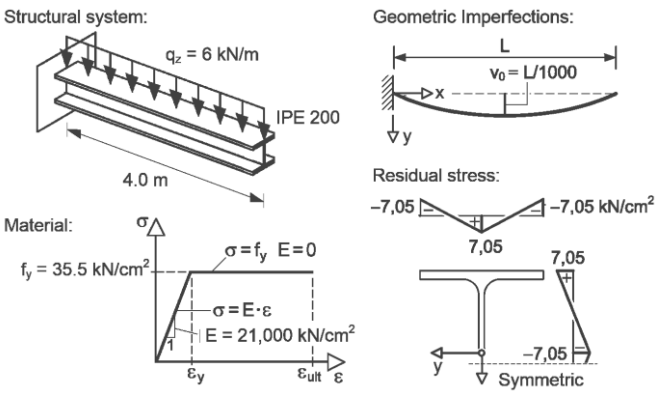

Figure 12 Internal forces and moments as well as degrees of freedom

Figure 12 shows the structural system and the calculation assumptions with regard to imperfections considered for present investigation. A linear-elastic ideal-plastic material behaviour is applied and linearly distributed residual stresses assumed. In line with common practice, geometric imperfections are accounted using a parabola bow imperfection with a maximum value of L/1000 [26]. It is worth mentioning that in the context of lateral torsional buckling, flexion in the predeformation is of decisive importance. With regard to the profile, rotation capacity is sufficient to allow plasticizing without encountering local buckling mechanisms.

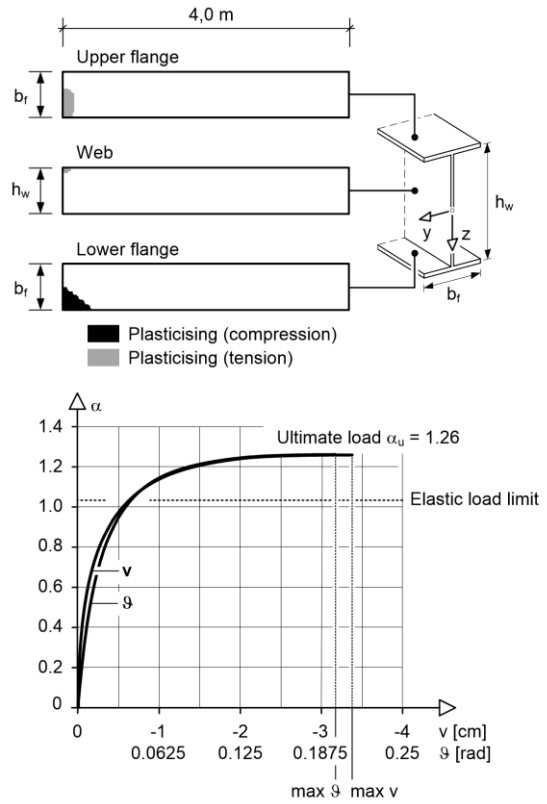

Figure 13 Internal forces and moments as well as degrees of freedom

Calculation results are displayed in Figure 13. The ultimate loading factor reaches $\alpha_{ult} = 1.26$, which gives a maximum load of $q_z = 1.26 \cdot 6 = 7.56\ kN/m$ and a corresponding bending moment at the restraint of $M_{b,Rk} = 60.48\ kN/m$. As can be seen, plasticising takes place at the restraint. However, the cross section capacity is not totally utilized and the capacity is determined by reaching the eigenvalue of the partially plasticized member. At the limit state, torsional rotations ϑ and lateral displacements v occur shown in the load-displacement-curves in Figure 13.

4.2 Resistance based on sophisticated FEM-model

Next to the calculations according to plastic zones theory, a sophisticated finite element model was also used to determine the member capacity (compare section 3.7). First the elastic critical loading factor was determined. For the IPE 200 - cantilever shown in Figure 12 with a length of 4.0 m the obtained value for the elastic critical moment is $M_{cr} = 69.09\ kNm$, i.e. very close to analytical results.

Considering geometrical and physical non-linearities, the member capacity is determined using two different approaches for imperfections. Applying a parabola shaped pre-deformation according to Figure 12 gives $M_{b,Rk} = 64.0\ kNm$. Including additional pre-stresses for capturing residual stresses reduces capacity to $M_{b,Rk} = 62.3\ kNm$ and if initial geometric imperfections are considered affine to the eigenmode, it is $M_{b,Rk} = 59.1 kNm$. The results show deviations of approximately 6% compared to the plastic zones theory.

4.3 Resistance based on reduction factor χ_{LT}

For reasons of comparison, the capacity of the example in Figure 12 is also analysed applying reduction factors presented in chapter 2. Cross section properties of the IPE 200 are tabled in [23] ($I_T = 6.846\ cm^4$, $I_\omega = 12{,}746\ cm^6$, $I_z = 142.4\ cm^4$, $M_{pl,y} = 78.33\ kNm$, class 1 section for pure bending). The elastic critical moment using a finite element calculation (FE-STAB) based on beam theory gives:

$$M_{cr} = 69.93\ kNm$$

Using the new Equations (19), (20), and (23), the elastic critical moment is determined with $\varepsilon_T = 5.76$, $k_1 = 10.9$, and $k_2 = -0.356$:

$$M_{cr} = \frac{10.9}{L}\sqrt{EI_z \cdot GI_T} \cdot (1 - 0.356) = 71.6\ kNm$$

With a deviation of 2.4%, good compliance of the presented approach for M_{cr} is again recognized compared to the numerical result. The non-dimensional slenderness and the reduction factor obtained using Equation (2) and (3) give $\bar{\lambda}_{LT} = \sqrt{78.33/71.6} = 1.05$ and $\chi_{LT} = 0.672$. This reduction factor is associated with the following moment capacity:

$$M_{b,Rk} = 0.672 \cdot 78.33 = 52.6\ kNm$$

In comparison to the capacity of the plastic zones theory calculation according to the previous section, this resistance is approximately 13% lower. However, χ_{LT} corresponds to a uniform moment distribution over beam length. This does not comply to the moment distribution in this example. Detailed information regarding the adjustment of χ_{LT} for the moment distribution of the regarded cantilever is not specified in EN 1993 though. As good approximation, $k_c \approx 1/1.33 = 0.752$ could be assumed, leading to $f = 0.891$ and $\chi_{LT,mod} = 0.754$. This gives

$$M_{b,Rk} = 0.754 \cdot 78.33 = 59.1\ kNm.$$

With respect to the plastic zones theory, the approximation now fits the numerical result by approximately 98%. In Table 3, the capacity of the member is determined analogously varying member length and comparing it to solutions of plastic zones theory. Good agreement is clearly recognized.

Table 3 Resistance of cantilever in Figure 11 with varying member length

	L [cm]	200	250	300	350	400
$M_{b,Rk}$[kNm]	$\chi_{LT,mod}$	75.11	71.28	67.26	63.15	59.06
	PZT	74.95	72.60	69.23	65.05	60.48
Deviation		-0.2%	1.8%	2.8%	2.9%	2.3%

PZT: Plastic zones theory

5 Conclusions

This paper deals with the structural behaviour of cantilever beams with uniformly distributed loads in terms of lateral torsional buckling. Approaches for approximating elastic critical moments are discussed. It is shown, that different practical formulae rely on same theoretical background. By comparing analytical approaches to solutions of numerical methods (FEM) based on beam theory, solution quality is investigated. In addition, the application of sophisticated numerical models is investigated with regard to the practical use in the context of EN1993. Finally, a new formula is derived for calculating elastic critical moments of cantilevers with distributed loads.

Afterwards, calculation of member capacity is exemplarily shown for cantilevers with distributed loads. Solution of EN 1993 is compared to solutions of plastic zones theory, i.e. numerical approaches, which will have increasing importance for the design of members in future, as possibilities for the application of these calculation procedures progress strongly.

References

[1] Trahair, N. S. (1993) *Flexural-Torsional Buckling of Structures*. E & FN Spon, an imprint of Chapman & Hall, London.

[2] Euler, L. (1759) *Sur la force des colonnes*. Mémoires Academic Royale des Sciences et Belle Lettres, Berlin, 13, partial translation by Van den Broek, J.A. (1947) American Journal of Physics, 15, 309-18.

[3] Michell, A. G .M. (1899) *Elastic stability of long beams under transverse forces*. Philosophical Magazine, 48, 298-309.

[4] Prandtl, L. (1899) *Kipperscheinungen*. Thesis, Munich.

[5] Timoshenko, S. P. (1953) *Einige Stabilitaetsprobleme der Elastizitaetstheorie*. In Collected Papers of Stephen P. Timoshenko, pp. 1-50, New York: McGraw-Hill.

[6] Timoshenko, S. P. (1953) *Sur la stabilité des systèmes élastiques*. In Collected Papers of Stephen P. Timoshenko, pp. 92-224, New York: McGraw-Hill.

[7] Chwalla, E. (1939) *Die Kippstabilität gerader Träger mit doppeltsymmetrischem I-Querschnitt*. Forschungshefte Stahlbau, H. 2, Berlin: Springer.

[8] Tolga Y., Nevzat K., Turab K. (2017) *Lateral-Torsional Buckling of European Wide Flange I-Section Beams.* Proceedings of the 2nd World Congress on Civil, Structural, and Environmental Engineering (CSEE'17).

[9] Hechtman, R.A., Hattrap, J.S., Styer, E.F. and Tiedmann, T.L. (1955) *Lateral buckling of rolled steel I-beams.* Proceedings, ASCE, 81 (Separate N. 797).

[10] Fukumoto, Y. and Kubo, M. (1977) *A survey of tests on lateral buckling strength of beams, in Preliminary Report*. 2nd International Colloquium on Stability of Steel Structures, ECCS-IABSE, Liege, pp. 233-40.

[11] Fukumoto, Y. and Kubo, M (1977) *A supplement to a survey of tests on lateral buckling strength of beams, in Final Report*. 2nd International Colloquium on Stability of Steel Structures, ECCS-IABSE, Liege, pp. 115-7.

[12] Fukumoto, Y. and Kubo, M. (1977) *An experimental review of lateral buckling of beams and girders*. In Proceedings, International Colloquium on Stability of Structures Under Static and Dynamic loads, SSRC-ASCE, Washington, pp. 541-62.

[13] EN 1993-1-1 (2009), Eurocode 3: Design of steel structures - Part 1-1: General rules and rules for buildings.

[14] Kraus, M., Kindmann, R. (2019) *Finite-Elemente-Methoden im Stahlbau*. 2nd Edition, Berlin: Verlag Ernst & Sohn, Wiley.

[15] Simoes R. (2014) *Design of Steel Building with worked examples*. 16-17 October, Brussels.

[16] Bureau, A. (2006) *NCCI: Elastic critical moment for lateral torsional buckling*. SN003a-EN-EU.

[17] Galea, Y. (2006) NCCI: *Elastic critical moment of cantilevers*. SN006a-EN-EU

[18] Kindmann, R. (2008) *Stahlbau Teil 2: Stabilität und Theorie II. Ordnung*. 4th Edition, Berlin: Verlag Ernst & Sohn, Wiley.

[19] Andrade A, Camotim D, Providencia e Costa P. (2007) *On the evaluation of elastic critical moments in doubly and singly symmetric I-section cantilevers*. J Construct Steel Res 63, p. 894–908.

[20] DIN 4114 (1952), Stabilitätsfälle (Knickung, Kippung, Beulung).

[21] ANSI/AISC 360-16 (2016), Specification for Structural Steel Buildings.

[22] Kraus, M. (2007) *On the Computation of Hot Rolled Cross Section Properties and Stresses using the Finite Element Method*. Proceedings of the 6th Int. Conference on Steel and Aluminium Structures (ICSAS'07), pp. 409-416.

[23] Kindmann, R., Kraus, M., Niebuhr, H. J. (2017) *Stahlbau Kompakt, Bemessungshilfen*, Profiltabellen. 4th Edition. Düsseldorf: Verlag Stahleisen.

[24] Ozbasaran H., Aydin R., and Dogan M. (2015) *An alternative design procedure for lateral-torsional buckling of cantilever I-beams*. Thin-Walled Struct., vol. 90, pp. 235-242, 2015.

[25] User Reference ANSYS© ,2019.

[26] Lindner, J., Scheer, J, Schmidt, H. (1998) Erläuterungen zur DIN 18800 Teil 1 bis Teil 4. Beuth Kommentrare, Berlin: Verlag Ernst & Sohn.

[27] Kindmann, R.; Kraus, M. (2019) *FE-Berechnungen mit Fließzonen für Tragfähigkeitsnach-weise nach DIN EN 1993-1-1 – Vereinfachte Berechnungsmethode für stabilitäts-gefährdete Bauteile*. Stahlbau 88, H. 4,S. 354-362.